Global NEST Journal, Vol 25, No 2, pp 44-49


# Photocatalytic degradation of reactive violet 1 by polyorthotoluidine/titanium dioxide nanocomposite

**Anjum M.N.*,+, Qasim S.+, Ahmad M.N., Iqbal S., Abrar S. and Nabi Z.**
Department of Applied Chemistry, Government College University Faisalabad 38000, Pakistan
Received: 09/02/2019, Accepted: 18/07/2022, Available online: 29/08/2022
*to whom all correspondence should be addressed: e-mail: anjumccj@hotmail.com
+ Anjum M.N. and Qasim S. have equal contributions
https://doi.org/10.30955/gnj.004281

**Graphical abstract**

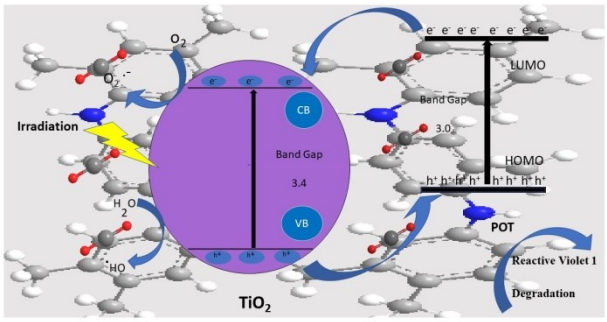


**Abstract**

Conducting poly(o-toluidine) (POT)/titanium dioxide ($TiO_2$) nanocomposite have been synthesized by in situ chemical oxidation polymerization of o-toluidine in the presence of $TiO_2$ nanoparticles. The various composites were synthesized by changing the percentage load of titanium dioxide nanoparticles in poly-ortho-toluidine matrix. The synthesized nanocomposites were characterized by using Scanning electron microscopy (SEM), X-Rays diffraction (XRD), and Fourier transform infrared spectroscopy (FTIR). The POT/$TiO_2$ nanocomposites were further employed to evaluate the photocatalytic potential of the composite materials towards reactive violet 1.

Keywords: photocatalytic degradation, nanocomposites, reactive violet 1, water pollution, dye degradation

## 1. Introduction

Among the natural resources water is most important necessity and is considered to be fundamental for existence of all living beings including human, economic development, and production of food. Now we require water conservation to save the globe and secure the future of humans. With the development of our lifestyle and civilization that is accomplishing new heights, now living organisms are paying a very big price for this development (Apostol *et al.,* 2012). Due to advancements in all fields such as in agriculture, industry, and new growing technologies are using more and more chemicals. Chemicals used in these industries have a great impact on the environment and contaminate the water (Al-Bastaki, 2004). Organic and inorganic chemicals used in industrial activities produce a large volume of contaminated water which causes hazardous health problems in humans and other living organisms (Behnajady *et al.,* 2006). There are many sources of chemicals such as dyes used in the paper industry, printing industry, food, and plastic industry. These industries are the main sources of colored substances in wastewater (Erfani and Javanbakht, 2018).

Many physical, biological, and chemical techniques have been used for the removal and degradation of dyes from wastewater (Liu *et al.,* 2007; Ahmad *et al.,* 2022). These techniques include separation by using membrane, chemical oxidation, adsorption, degradation using microbes, electrochemical method, photocatalytic method, and coagulation. These all techniques have very good outcomes and are widely used all over the world for dye removal (Rafiee *et al.,* 2020; Mobin and Tanveer, 2012; Ahmad *et al.,* 2020).

In the advanced oxidation process, photocatalysis is an emerging and efficient method for the treatment of several dyestuffs. In this process, $TiO_2$, and CdS have the most commonly studied photocatalysts (Campos *et al.,* 2019). But among the various materials used for photocatalysis, $TiO_2$ is the finest photocatalyst, which is extensively utilized for the photcatalytic degradation of dye (Ullah and Dutta, 2008; Tang *et al.,* 2021; Nadeem *et al.,* 2018).

For the surface modification of $TiO_2$, different physical and chemical methods have been utilized for $TiO_2$ particles (Jamil and Fasehullah, 2021). The most important and efficient method for surface modification is the wrapping of $TiO_2$ particles as core by the polymeric shell using conducting polymers under visible light irradiation, their photocatalytic performance has been investigated against different chemicals (Khan *et al.,* 2020; Neppolian *et al.,* 2002; Rafiee *et al.,* 2020; Zan *et al.,* 2004; Anjum *et al.,* 2014). The conducting polymers enhance the photocatalytic potential of $TiO_2$ by circulating the free electrons (Shehzad *et al.,* 2016; Shehzad *et al.,* 2014). Polyorthotoluidine is one of the extensively used

conducting polymers because of its cheap production cost, stability, ease to prepare, and reversible acid-base chemistry, (Konstantinou and Albanis, 2004; Olad and Nosrati, 2012; Hussain *et al.,* 2018; Ahmad *et al.,* 2018). In the current study, the POT/$TiO_2$ nanocomposites was tested for the photocatalytic degradation of dye (reactive violet 1) in aqua media under ultraviolet irradiation.

## 2. Materials and methods

### *2.1. Chemicals*

o-Toluidine monomer, potassium persulphate (KPS), hydrochloric acid, and titanium dioxide (~50 nm) were procured from Sigma Aldrich used as received and Methanol acetic acid.

### *2.2. Synthesis of $TiO_2$ NPs*

The acetic acid hydrolysis approach was used to prepare $TiO_2$ nanoparticles. The solution of acetic acid (1M) was prepared by using distilled $H_2O$ under continuous stirring for 30 minutes then, 0.5M solution of titanium isopropoxide was poured into the acidic solution and stirred at 50 °C for 6 hours. A greyish-colored material was formed. That was separated by centrifuge and dried a room temperature (Zhou *et al.,* 2016).

### *2.3. Regeneration of $TiO_2$*

$TiO_2$ nanoparticles were regenerated by adding 10g $TiO_2$ in 20 ml of 0.1M $HNO_3$ solution under continuous stirring by a magnetic stirrer for 24 hours. Then it was sonicated for 2 hours to prevent agglomeration. Finally, it was separated and dried at 70 °C in an electric oven.

### *2.4. Synthesis of POT/$TiO_2$ nanocomposites*

POT/$TiO_2$ nanocomposites were synthesized in three different compositions which are mentioned in (Table 1).

**Table 1.** Compositions of POT/$TiO_2$

| Sample name | POT | $TiO_2$ | Ratio |
|---|---|---|---|
| Composition 1 (S1) | 2ml | 10g | 1:5 |
| Composition 2 (S2) | 2ml | 5g | 2:5 |
| Composition 3 (S3) | 2ml | 20g | 1:10 |

First of all, 1 molar solution of HCl was prepared by diluting the concentrated HCl by using the dilution formula. Three different samples (S1, S2, & S3) were prepared by loading the $TiO_2$ NPs (10g, 5g, & 20g) in the POT matrix, respectively (Anwar *et al.,* 2015). Then, 100 ml of 1M HCl was taken in a beaker and $TiO_2$ powder was dispersed in it by magnetic stirring for 30 minutes. After that, 2 ml of ortho-toluidine was added to the acidic solution. Then, another solution comprising 25 ml of distilled water and 5g of potassium persulphate (KPS) was prepared. The KPS solution was added into the monomer solution and the reaction mixture was allowed to polymerize under constant stirring for 3 hours at room temperature. After 3 hours of constant stirring, a blackish green colored gel was obtained. The sample was then separated by centrifugation at 4000 rpm for 5 minutes. The sample was washed several times with water then with ethanol for complete removal of solvent and impurities. The sample was dried in an electric oven at 80 °C for 2 hours. Similarly, other samples were prepared by varying the amount of $TiO_2$ NPs. After that obtained solid is converted into a fine powder which is POT/$TiO_2$ nanocomposite. The samples have further proceeded for characterization.

## 3. Results and discussion

### *3.1. Fourier-transform Infrared Spectroscopy (FTIR)*

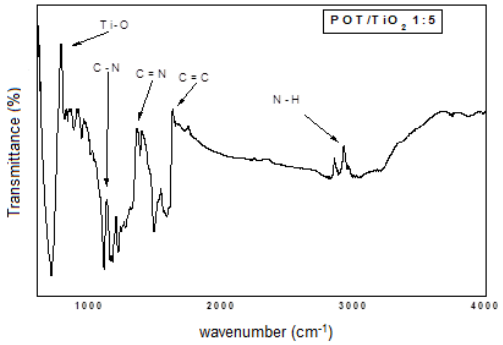


**Figure 1.** FT-IR spectrum of POT/$TiO_2$ sample (S1).

The FT–IR spectrum of sample S1 of POT/$TiO_2$ nanocomposite was presented in (Figure 1). The FT–IR spectrum showed a vibrational peak at 711 $cm^{-1}$ due to the presence of Ti–O bond (Zhou *et al.,* 2016). The wide peak at 3032 $cm^{-1}$ and 2882 $cm^{-1}$ was associated with N–H stretching vibration. The peaks at 1487 $cm^{-1}$ and 1585 $cm^{-1}$ exhibited C=N and C=C stretching vibrations for the benzenoid and quinoid structures. While the signal at 1382 $cm^{-1}$ indicated that the benzenoid units were in the C–N stretching phase. The signal in the spectrum at 882 $cm^{-1}$ was allocated to the out of plane C–H vibrational mode which confirmed the formation of POT/$TiO_2$ (Zan *et al.,* 2004).

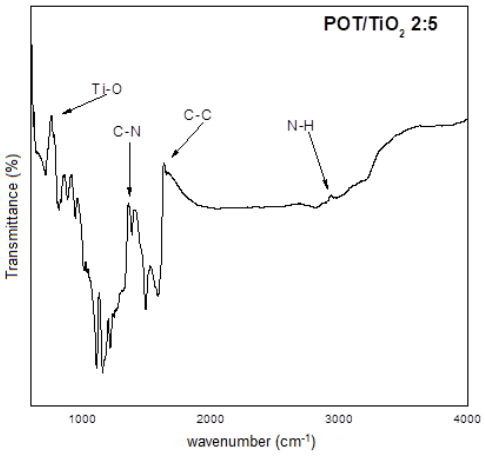


**Figure 2.** FT-IR spectrum of POT/$TiO_2$ sample (S2).

The FTIR spectrum of POT/$TiO_2$ nanocomposite was shown in (Figure 2). Due to the Ti–O vibrations, the FT–IR spectrum displayed a peak at 710 $cm^{-1}$. The peaks observed in the spectrum, at 1488 $cm^{-1}$ and 1586 $cm^{-1}$, showed the C–C stretching vibration of the benzenoid and quinoid structure respectively. Moreover, aromatic amine contain C-N stretching was showed peak at 1382 $cm^{-1}$. The out of plane and in-plane C–H bending modes were given to the peaks that emerged at 812 cm-1 and 1154 cm-1,

respectively. The peak detected at 1213 $cm^{-1}$ indicated the N–H bond of an amine of the aromatic ring (Konstantinou and Albanis, 2004; Pham *et al.,* 2022).

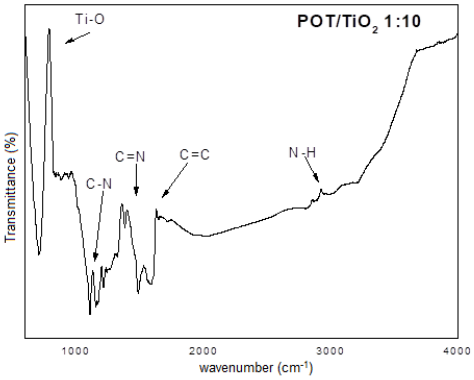


**Figure 3**. FT-IR spectrum of POT/$TiO_2$ sample (S3).

The FT–IR spectrum of sample S3 of POT/$TiO_2$ nanocomposite was given in (Figure 3). The FT–IR spectrum showed a broad peak at 706 $cm^{-1}$ due to Ti–O vibrations. And all other peaks were the same as for samples S1 and S2. This proved the formation of POT/$TiO_2$ nanoparticles.

In spectra of POT/$TiO_2$ nanocomposites, most of the peaks for POT were observed as reported (Gayathri and Balan, 2019; Shehzad *et al.,* 2013) except a peak at 1161.70 $cm^{-1}$, this peak was slightly changed its position and shifted to 1174 $cm^{-1}$ for the spectra of POT/$TiO_2$ nanocomposites. This shifting of peak confirmed that delocalization was greater due to the full contact between the $TiO_2$ nanoparticles and the POT matrix. Consequently, it is concluded that the shifting of peaks to some extent was due to the interaction of POT and $TiO_2$ nanoparticles in composite materials (Shakir *et al.,* 2014).

*3.2. Scanning Electron Microscopy (SEM)*

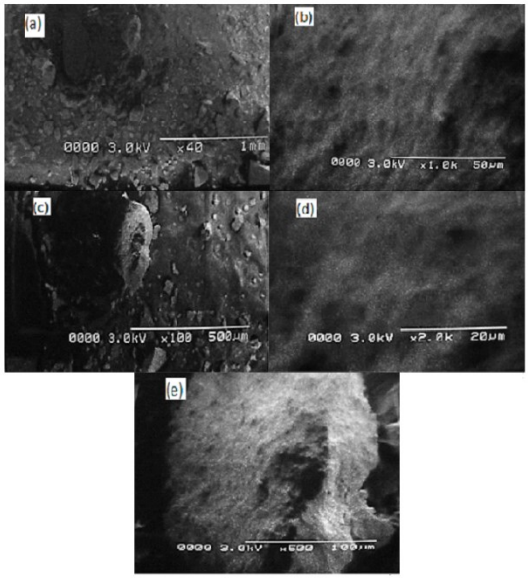


**Figure 4.** SEM images of POT/$TiO_2$ nanocomposite Sample (S1).

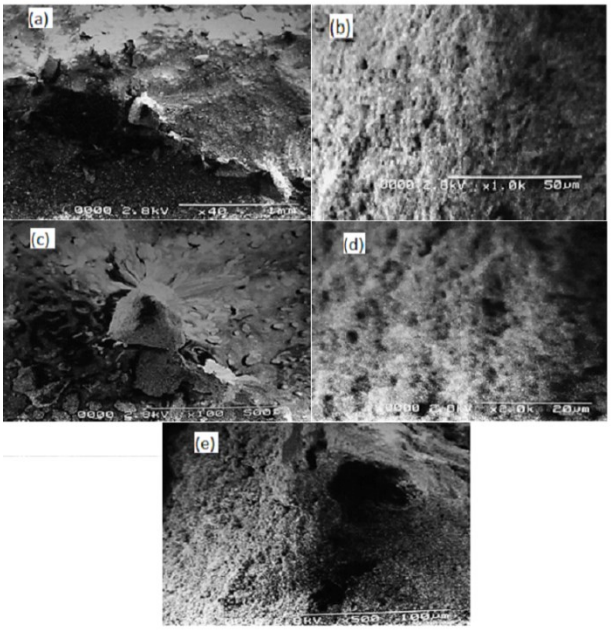


**Figure 5.** SEM images of POT/$TiO_2$ nanocomposite Sample (S2).

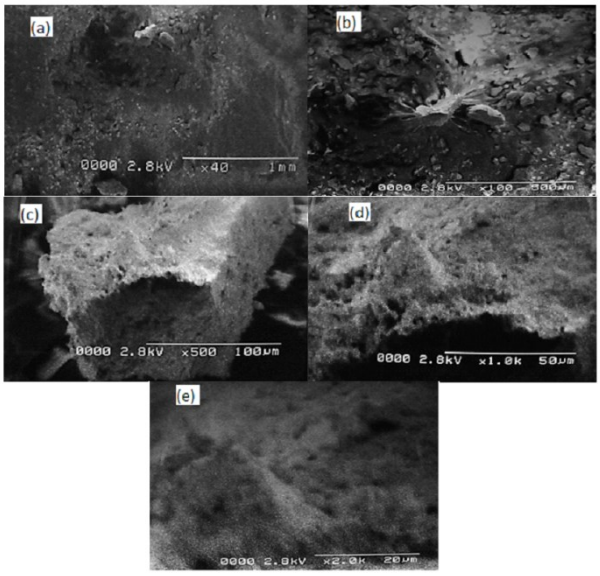


**Figure 6.** SEM images of POT/$TiO_2$ nanocomposite Sample (S3).

The SEM images of all 3 samples (S1, S2, S3) labeled on (Figure 4–6) showed the structure characteristics and morphologies of POT/$TiO_2$ nanocomposite. The white spots showed the presence of $TiO_2$ in all 3 figures. In Figure 4, the spreading of $TiO_2$ nanoparticles was observed throughout the POT matrix. These images showed the core-shell structure of the nanocomposite. Irregular clusters were shown in these images which indicated the uniform diffusion of titanium dioxide nanoparticles in the matrix of polyorthotoluidine. These figures also showed the porous morphology which explained the adsorption properties of the polymer. It also exhibited a granular structure (Matei *et al.,* 2008). In Figure 4 (d), there was a large granule collection on the POT/$TiO_2$ nanocomposite (Zan *et al.,* 2004; Hussain *et al.,* 2017). In other images of SEM 5 and 6 similar features were observed for S2 and S3 in the respective figures.

*3.3. X-ray diffraction analysis*

XRD technique is used to determine the structure of different nanocomposites. POT/$TiO_2$ nanocomposite structures have been examined by using X-ray diffraction. To identify the sample's phase and crystallinity, XRD measurements were recorded. Figure 7 showed the XRD outlines of the POT/$TiO_2$ composite. The XRD pattern of the POT/$TiO_2$ NC for sample S1 showed the different peaks whose values of 2θ° were given as: 26.2, 37.1, 39.2, 42.4, 44.1, 55.3, 56.7, 66.8, 67.1, 69.0, and 69.8. That resembled the diffractions of (110), (101), (200), (111), (210), (211), (220), (002), (310), (221) and (301) facets of the $TiO_2$ rutile phase. It was observed that the results of the prepared nanocomposite were in accordance with the findings given by (Liu *et al.,* 2007). In Figure 7(a), two wide peaks for POT were observed at the value of 2θ°= 5–40 and it was maximum at around 27. Most of the peaks in the spectra became weaker but were in good agreement with them as compared with their pure counterparts. The decreasing intensity in the XRD pattern of sample S1 at 25 could be the inclusion of inorganic particles (Liu *et al.,* 2004).

The X-ray patterns of POT/$TiO_2$ nanocomposites of sample S2 were shown in Figure 7(b). The study on X-ray patterns showed different characteristic peaks which were observed in spectra at 2θ°= 28, 34, 44, 55, 58, and 64, etc. In spectra, the peak at 2θ° = 25 is for POT that is expected to appear in POT/TiO2 nanocomposite. The $TiO_2$ nanoparticle size also influenced the crystallite size of the whole nanocomposite. The order of POT < POT/$TiO_2$ could be owing to the polymerization of *o*-toluidine monomers on $TiO_2$ surface, encasing $TiO_2$ nanoparticles. (Shakir *et al.,* 2014).

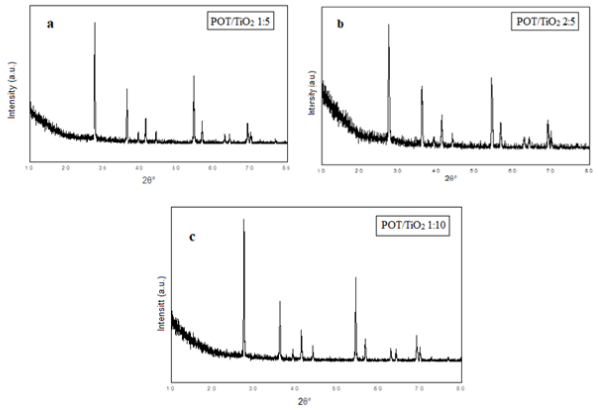


**Figure 7.** XRD pattern of POT/$TiO_2$ sample (S1).

XRD pattern showed four different peaks in the region of 2θ°= 16-26° in Figure 7(c), where the largest peak was round 2θ°= 18.1°. It was imputed that the polymer chains of polyamine were perpendicular, parallel, and repeated after several distances. The second peak present at 2θ°= 20° was also characteristic. It indicated the close contact between the chains. Additionally, the peak present at 2θ°= 24° indicated that the polyorthotoluidine had a very small degree of crystallinity and polyorthotoluidine chains were scattered in the spaces present between the planes. The XRD pattern of the polyorthotoluidine/titanium dioxide nanocomposite indicated that there were very small peaks of titanium dioxide nanoparticles at 2θ°= 32- 38°. These peaks indicated that the molar ratio was very small as compared to polyaniline. The peak at 2θ°= 32.5° explained the crystallinity and wurtzite hexagonal structure of titanium dioxide (Huang *et al.,* 2007; Shehzad *et al.,* 2016).

## 4. Photocatalytic Activity

To investigate the catalytic efficiency of prepared POT/$TiO_2$ nanocomposites, a local device was used which had two components. The first was a degradation box and the second was a Xe arc-lamp of 500W. By using this device, the nanocomposites photocatalytic performance was assessed. To study the degradation activity, 100 ml solutions (5mg/L) of dye were prepared in a glass test tube. Then 0.1g of the sample catalyst was added to the dye solution. Keeping the light source off, dye solution was placed in the degradation box. To achieve the equilibrium, the sample dye solution (reactive violet 1) was kept in the degradation box for 1 h under dark and then the dye sample was taken out from the degradation box. The discoloration of dye samples was analyzed using a UV-vis spectrophotometer. Then sample dye solution was placed in a degradation box in the presence of ultraviolet irradiation and the same experiment was carried out. The distance between the sample of dye solution and the light source was kept at 16 cm. The discoloration dye sample was analyzed at different time intervals and by using a spectrophotometer (Abdel-Mottaleb *et al.,* 2019; Anwar *et al.,* 2017; Hussain *et al.,* 2019) (Figure 8).

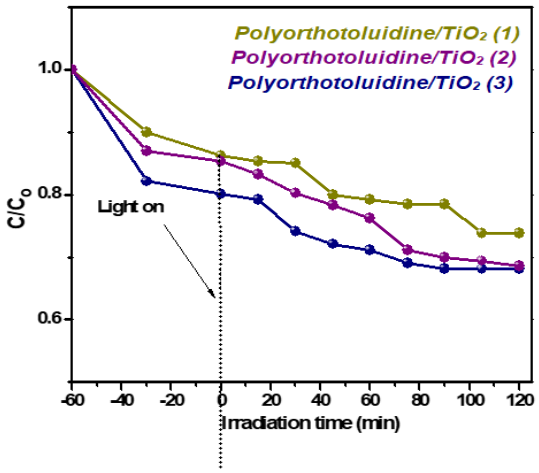


**Figure 8.** Photocatalytic degradation curve.

The degradation of reactive violet 1 under visible and ultraviolet light was examined by the prepared nanocomposite (S1). This degradation of dye was checked after a different interval of time under visible and ultraviolet light as shown in (Figure 9). Intensities of dye absorption band were decreased which showed that dye was degraded continuously. It was observed that after 110 minutes there was 26 percent of dye was degraded by the nanocomposite (S1) and after that degradation process was slowed down as shown in (Figure 9).

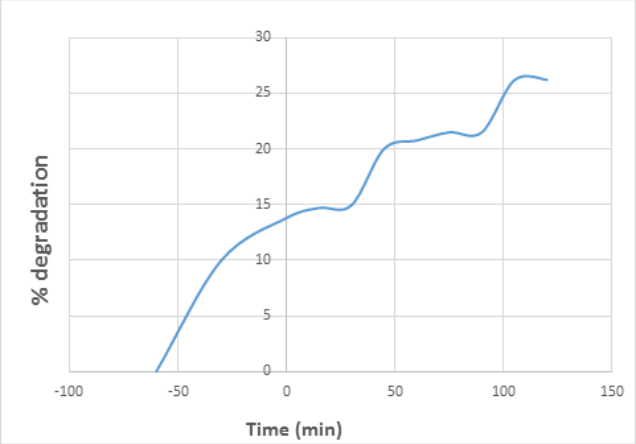


**Figure 9.** Percentage degradation efficiency of POT/$TiO_2$ (S1).

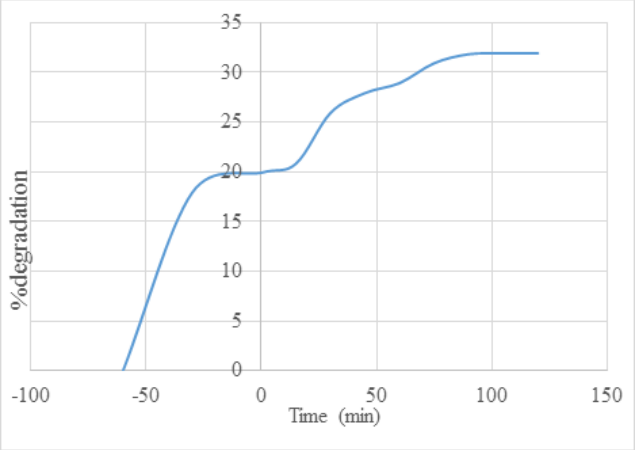


**Figure 10.** Percentage degradation efficiency of POT/$TiO_2$ (S2).

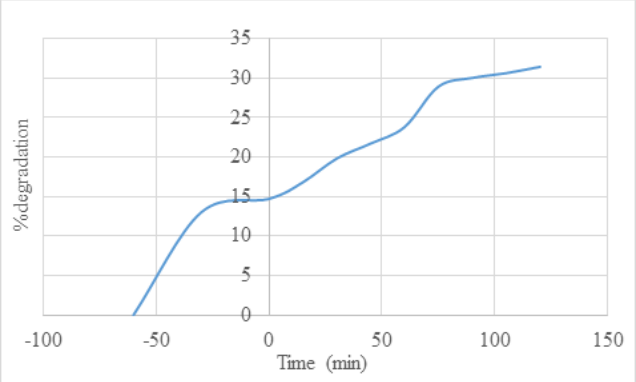


**Figure 11.** Percentage degradation efficiency of POT/$TiO_2$ (S3).

The degradation of reactive violet 1 under visible and ultraviolet light was examined by another prepared nanocomposite (S2). This degradation of dye was checked after a different interval of time under visible and ultraviolet light as shown in (Figure 10). Intensities of dye absorption band were decreased which shows that dye was degraded continuously. It was observed that after 110 min there was 31 percent of dye was degraded by the nanocomposite (S2) after that degradation process was slowed down as shown in (Figure 10).

The degradation of reactive violet 1 under visible and ultraviolet light was examined by another prepared nanocomposite (S3). This degradation of dye was checked after different intervals of time under visible and ultraviolet light as shown in (Figure 11). Intensities of dye absorption band were decreased which showed that dye was degraded continuously. It was observed that after 110 minutes 32 percent of dye was degraded by the nanocomposite (S3) and after that degradation process was slowed down as shown in (Figure 11).

## 5. Conclusion

In summary, POT/$TiO_2$ nanocomposites were prepared successfully by using chemical oxidative polymerization techniques. The different analytical approaches were used to confirm the structure and morphology of the produced nanocomposites. The degradation of reactive violet 1 was evaluated under ultraviolet irradiation. The reactive violet 1 degradation was directly related to the amount of $TiO_2$ in the composite material. The results showed a better potential to degrade reactive violet 1 and other reactive dyes for environmental application.

### References

Abdel-Mottaleb M., Khalil A., Karim S., Osman T., and Khattab A. (2019). High performance of PAN/GO/ZnO composite nanofibers for photocatalytic degradation under visible irradiation. *Journal of the Mechanical Behavior of Biomedical Materials,* **96**, 118–124.

Ahmad M.N., Hussain A., Anjum M.N., Hussain T., Mujahid A., Khan M.H., and Ahmed T. (2020). Synthesis and characterization of a novel chitosan-grafted-polyortho-ethylaniline biocomposite and utilization for dye removal from water. *Open Chemistry*, **18**(1), 843–849.

Ahmad M.N., Nadeem S., Javed M., Iqbal S., Khan M., Alsaab H.O., and Mohyuddin A. (2022). Photocatalytic Degradation of Yellow-50 Using Zno/Polyorthoethylaniline Nanocomposites. *Journal of the Minerals,* 1–7.

Ahmad M.N., Rafique F., Nawaz F., Farooq T., Anjum M.N., Hussain T., and Shehzad K. (2018). Synthesis of antibacterial poly (o-chloroaniline)/chromium hybrid composites with enhanced electrical conductivity. *Chemistry Central Journal*, **12**(1), 1–7.

Ahmad S., Riaz U., Kashif M., and Khan M.S. (2012). Development of Nanostructured Poly (o-toluidine) Reinforced Organic-Inorganic Hybrid Composites. *Journal of Inorganic and Organometallic Polymers and Materials,* **22**(3), 662–670.

Al-Bastaki N. (2004). Removal of methyl orange dye and $Na_2SO_4$ salt from synthetic wastewater using reverse osmosis. *Chemical engineering and processing: Process Intensification,* **43**(12), 1561–1567.

Anjum M.N., Zia K.M., Zhu L., Ahmad M.N., Zuber M., and Tang H. (2014). Adsorption of methyl orange using self-assembled porous microspheres of poly (o-chloroaniline). *Korean Journal of Chemical Engineering*, **31**(12), 2192–2197.

Anwar T., Wang L., Tongxiang L., He X., Sagar R.U.R., and Shehzad K. (2015). Effect of aspect ratio of titanium dioxide nanotube arrays on the performance of lithium ion battery. *International Journal of Electrochemal Science*, **10**(7), 6537–6547.

Anwar T., Li W., Sagar R.U.R., Nosheen F., Singh R., Jafri H. M., and Tongxiang L. (2017). Cathodic titania nanotube arrays as anode material for lithium-ion batteries. *Journal of materials science*, **52**(8), 4323–4332.

Apostol L. C., Pereira L., Pereira R., Gavrilescu M., and Alves M.M. (2012). Biological decolorization of xanthene dyes by anaerobic granular biomass. *Biodegradation,* **23**(5), 725–737.

Behnajady M., Modirshahla N., and Hamzavi R. (2006). Kinetic study on photocatalytic degradation of CI Acid Yellow 23 by

ZnO photocatalyst. *Journal of Hazardous Materials,* **133**(1–3), 226–232.

Campos A.F.C., Michels-Brito P.H., da Silva F.G., Gomes R.C., Gomide G., and Depeyrot J. (2019). Removal of direct yellow 12 from water using CTAB coated core-shell biomagnetic nano adsorbents. *Journal of Environmental Chemical Engineering,* **7**(2), 103031.

Erfani M., and Javanbakht V. (2018). Methylene Blue removal from aqueous solution by a biocomposite synthesized from sodium alginate and wastes of oil extraction from almond peanut. *International Journal of Biological Macromolecules,* **114**, 244–255.

Gayathri V., and Balan R. (2019). Synthesis and Characterization of Polyorthotoluidine doped with commercial $TiO_2$ nanoparticle. *J. Environ. Nanotechnol*, **8**(3), 30–33.

Huang Y.H., Hsueh C.L., Huang C.P., Su L.C., and Chen C.Y. (2007). Adsorption thermodynamic and kinetic studies of Pb (II) removal from water onto a versatile $Al_2O_3$ supported iron oxide. *Separation and Purification Technology,* **55**(1), 23–29.

Hussain A., Ahmad M.N., Jalal F., Yameen M., Falak S., Noreen S., and Iqbal M. (2019). Investigating the Antibacterial Activity of POMA Nanocomposites. *Polish Journal of Environmental Studies*, **28**(6).

Hussain T., Ahmad M.N., Nawaz A., Mujahid A., Bashir F., and Mustafa G. (2017). Surfactant incorporated Co nanoparticles polymer composites with uniform dispersion and double percolation. *Journal of Chemistry*, *2017*.

Hussain T., Jabeen S., Shehzad K., Mujahid A., Ahmad M.N., Farooqi Z.H., and Raza M.H. (2018). Polyaniline/silver decorated-MWCNT composites with enhanced electrical and thermal properties. *Polymer Composites*, **39**(S3), E1346–E1353.

Jamil S., and Fasehullah M. (2021). Effect of Temperature on Structure, Morphology, and Optical Properties of $TiO_2$ Nanoparticles. *Materials Innovations,* **1**(1), 22–29.

Khan A.A., and Baig U. (2013). Electrical conductivity and humidity sensing studies on synthetic organic-inorganic Poly-o-toluidine–titanium (IV) phosphate cation exchange nanocomposite. *Solid-State Sciences,* **15**, 47–52.

Khan J.A., Sayed M., Shah N.S., Khan S., Zhang Y., Boczkaj G., Dionysiou D.D. (2020). Synthesis of eosin modified $TiO_2$ film with co-exposed {001} and {101} facets for photocatalytic degradation of para-aminobenzoic acid and solar $H_2$ production. *Applied Catalysis B: Environmental,* **265**, 118557.

Konstantinou I.K., and Albanis T.A. (2004). $TiO_2$ assisted photocatalytic degradation of azo dyes in aqueous solution: Kinetic and mechanistic investigations: A review. *Applied Catalysis B: Environmental,* **49**(1), 1–14.

Liu C.H., Wu J.S., Chiu H.C., Suen S.Y., and Chu K.H. (2007). Removal of anionic reactive dyes from water using anion exchange membranes as adsorbers. *Water Research,* **41**(7), 1491–1500.

Liu G., Wang J., Zhu Y., and Zhang X. (2004). Destructive adsorption of carbon tetrachloride on nanometer titanium dioxide. *Physical Chemistry Chemical Physics,* **6**(5), 985–991.

Matei A., Cernica I., Cadar O., Roman C., and Schiopu V. (2008). Synthesis and characterization of ZnO polymer nano-composites. *International Journal of Material Forming,* **1**(1), 767–770.

Mobin M., and Tanveer N. (2012). Corrosion performance of chemically synthesized poly (aniline-co-o-toluidine) copolymer coating on mild steel. *Journal of Coatings Technology and Research,* **9**(1), 27–38.

Nadeem Ahmad M., Anjum M.N., Nawaz F., Iqbal S., Saif M.J., Hussain T., and Shehzad K. (2018). Synthesis and antibacterial potential of hybrid nanocomposites based on polyorthochloroaniline/copper nanofiller. *Polymer Composites*, **39**(12), 4524–4531.

Neppolian B., Choi H., Sakthivel S., Arabindoo B., and Murugesan V. (2002). Solar light-induced and $TiO_2$ assisted degradation of textile dye reactive blue 4. *Chemosphere,* **46**(8), 1173–1181.

Olad A., and Nosrati R. (2012). Preparation, characterization, and photocatalytic activity of polyaniline/ZnO nanocomposite. *Research on Chemical Intermediates,* **38**(2), 323–336.

Pham P.V., Bodepudi S.C., Shehzad K., Liu Y., Xu Y., Yu B., and Duan X. (2022). 2D Heterostructures for Ubiquitous Electronics and Optoelectronics: Principles, Opportunities, and Challenges. *Chemical Reviews*, **122**(6), 6514–6613.

Rafiee E., Pami N., Zinatizadeh A.A., and Eavani S. (2020). A new polyoxometalate/$TiO_2$ nanocomposite for efficient visible photodegradation of dye from wastewater, liquorice, and yeast extract: Photoelectrochemical, electrochemical, and physical investigations. *Journal of Photochemistry and Photobiology A: Chemistry,* **386**, 112145.

Shakir M., Khan M.S., Al Resayes S.I., Baig U., Alam P., Khan R.H., and Alam M. (2014). In vitro DNA binding, molecular docking, and antimicrobial studies on a newly synthesized poly (o-toluidine)/titanium dioxide nanocomposite. *RSC Advances,* **4**(74), 39174–39183.

Shehzad K., Dang Z.M., Ahmad M.N., Sagar R.U.R., Butt S., Farooq M.U., and Wang T.B. (2013). Effects of carbon nanotubes aspect ratio on the qualitative and quantitative aspects of frequency response of electrical conductivity and dielectric permittivity in the carbon nanotube/polymer composites. *Carbon*, **54**, 105–112.

Shehzad K., Ahmad M.N., Hussain T., Mumtaz M., Shah A.T., Mujahid A., and Dang Z.M. (2014). Influence of carbon nanotube dimensions on the percolation characteristics of carbon nanotube/polymer composites. *Journal of Applied Physics*, **116**(6), 064908.

Shehzad K., Hussain T., Shah A.T., Mujahid A., Ahmad M.N., Anwar T., and Ali A. (2016). Effect of the carbon nanotube size dispersity on the electrical properties and pressure sensing of the polymer composites. *Journal of Materials Science*, **51**(24), 11014–11020.

Shehzad K., Xu Y., Gao C., and Duan X. (2016). Three-dimensional macro-structures of two-dimensional nanomaterials. *Chemical Society Reviews*, **45**(20), 5541–5588.

Tang Z., Lu Y., Hou Y., Mushtaq A., Farheen J., Ali I., and Kong X. (2021). Synthesis of Biocompatible $Fe_3O_4$–$TiO_2$ Janus Nanocomposites for T2 Magnetic Resonance Imaging and Photodynamic Therapy of Cancer In Vitro. *Materials Innovations*, **1**(2), 2–11.

Ullah R., and Dutta J. (2008). Photocatalytic degradation of organic dyes with manganese doped ZnO nanoparticles. *Journal of Hazardous Materials,* **156**(1–3), 194–200.

Zan L., Tian L., Liu Z., and Peng Z. (2004). A new polystyrene/$TiO_2$ nanocomposite film and its photocatalytic degradation. *Applied Catalysis A: General,* **264**(2), 237–242.

Zhou T., Xie X., Cai J., Yin L., and Ruan W. (2016). Preparation of poly (o-toluidine)/$TiO_2$ nanocomposite films and application for humidity sensing. *Polymer Bulletin,* **73**(3), 621–630.